Title

Numerical modeling study of a man-made low-permeability barrier for the compressed air energy storage in high-permeability aquifers

Authors

Li, Yi
Pan, Lehua
Zhang, Keni
et al.

Publication Date

2017-12-01

DOI

10.1016/j.apenergy.2017.09.065

Peer reviewed

Numerical modeling study of a man-made low-permeability barrier for the compressed air energy storage in high-permeability aquifers

Yi Li[a] Lehua Pan[b] Keni Zhang[c] Litang Hu[a] Jinsheng Wang[a] Chaobin Guo[d]

Abstract

Compressed air energy storage (CAES) is a grid-scale energy storage technology for intermittent energy, as proven by the decades-long successful operation of two existing compressed air energy storage in cavern (CAESC) power plants. Because of the limited availability of salt domes appropriate for CAESC, the more widely available aquifers (compressed air energy storage in aquifers, CAESA) have recently attracted considerable attention as candidates for CAES. An ideal aquifer for CAESA is highly permeable around the well to facilitate easy injection and withdrawal of air, but the high-permeability region is surrounded by low-permeability zones to minimize the loss of injected air and decrease in energy efficiency. However, such ideal geological structures are not always available in nature. Therefore, the potential of creating man-made low-permeability barrier in high-permeability aquifers is very interesting. In this paper, we investigate the feasibility of man-made low-permeability barriers in high-permeability aquifers using the numerical simulator TOUGH2/Gel to calculate the three-component flow (including a miscible gelling liquid). The simulation results show that an expected low-permeability barrier can be created by injecting grout with certain properties, and the altered aquifer performs well for CAESA. Additional sensitivity studies are also performed to reveal the effects of the various factors on the success of the low-permeability barrier creation, including the critical solidification concentration, the scale factor of the time dependence of the grout viscosity, the relative density of the grout, and the volume of the follow-up water injection. The results indicate that, in a horizontal aquifer, low critical solidification concentrations, and small scale factors are generally preferred and the density of grout should be close to that of the in situ water. For the given volume of the injected grout, there is an optimal follow-up water injection that will create the largest storage space without damaging the barrier. These results may help to extend the candidate sites for CAESA and the prospect of large scale energy storage.

Keywords: Compressed air energy storage, High-permeability aquifer, Man-made low- permeability barrier, Energy efficiency, Model

Nomenclature

α1

coefficients of exponential Gel Time Curve

α3

coefficients of exponential Gel Time Curve

μl
: mixing liquid viscosity (Pa s)

Xlgel
: mass fraction of gel in the liquid phase

Sl
: saturation of liquid

ϕ∗
: porosity of altered porous medium

k∗
: permeability of altered porous medium

k
: permeability of origin porous medium

m
: exponent of Power-law Permeability Reduction Model

b
: exponent of Power-law mixing rule

h
: aquifer thickness (m)

ρ_w
: density of water (kg/m^3)

ρ_g
: density of grout (kg/m^3)

r_{bc}
: center of ideal barrier (m)

r_{po}
: outer boundary of ideal barrier (m)

Eefficiency
: round-trip energy efficiency

Einjection
: energy injected through wellhead

Rwmass
: ratio of liquid water mass production

Mwmass-p
: liquid water mass production (kg)

α2
: coefficients of exponential Gel Time Curve

μgel
: pure grout viscosity (Pa s)

μw
: pure water viscosity (Pa s)

Xcritical
: critical solidification concentration

Sg
: saturation of gas

ϕ
: porosity of original porous medium

krg
: relative permeability of gas

γ
: scaling factor for Gel Time Curve

t_g
: injection grout duration (s)

t_w
: water injection duration (s)

q_w
: water injection rate (kg/s)

q_g
: grout injection rate (kg/s)

r_{bl}
: lowest permeability distance (m)

r_{pi}
: inner boundary of ideal barrier (m)

$r_{o\text{-}I}$
: width of ideal barrier (m)

Eproduction

energy produced through wellhead

Rgmass

ratio of gas mass production

Mgmass-p

gas mass production (kg)

Mtotal-p

total mass production (kg)

1. Introduction

Wind energy and solar energy can be considered potential clean, sustainable energy sources of the future. However, the wide adoption of wind and solar energy, which are inherently intermittent energy sources, requires grid-scale energy storage technologies. CAES (compressed air energy storage) has been verified as an effective and low-cost grid storage technology [1], [2]. The Huntorf plant (290 MW) in Germany and the McIntosh plant (110 MW) in USA have been successfully operated for decades [3], [4]. The performance of CAES has been studied with respect to many factors, which include the temperature and pressure variance of air in the cycle operation process [5], the heat transfer coefficient between cavern walls and the air impact on energy storage [6], and the dynamic behaviors in the adiabatic CAES plant [7], [8]. However, the limit of storage space, such as in the salt-dome structure of the Huntorf and McIntosh plants, has hindered the wide expansion of the CAES technology in the industry.

Recently, CAESA (compressed air energy storage in aquifers) has been proposed and studied because aquifers are more widely available than salt domes. In addition, the cost of CAESA could be as low as 0.11 $/KW h which is more attractive than the cost of CAESC (compressed air energy in caverns) (2 $/KW h) [9]. Some theoretical studies using numerical simulation methods have investigated the feasibility of CAESA. Kushnir et al. analyzed the air pressure variance in an anisotropic aquifer and suggested that the air layer height and discharge period are important factors in the control of water coning [10]. Oldenburg and Pan developed the coupled wellbore-reservoir model to investigate the CAES in porous media and found that the permeability, sealing characteristics and size impact the system performance [11]. Using the TOUGH2/EOS3 module, Guo et al. investigated the impact of including uniform aquifer permeability, geological structures and injection parameters on the system cycle times (i.e., the times a given system, with a given gas bubble, can sustain balanced injection-production cycles). Their study showed that for a uniform aquifer, too high permeability will be a disadvantage because it causes more loss of injected air and energy and thus decreases the system cycle times whereas too low permeability will also be a disadvantage because it limits the production rate [12]. The

performances of CAESC and CAESA have been compared and indicate that the CAESA has satisfactory energy storage efficiency if the high-permeability aquifer is surrounded by a low-permeability barrier [13], [14]. Favorable geological structures can be found in nature, e.g., a sand lens embedded in a clay formation, a high-permeability block enclosed by low-permeability blocks due to fault offset, or a dome structure (Fig. 1, upper panels), although they are not widely available. For the idealized system depicted in Fig. 1 (lower panel), the high-permeability block (k1 = 10 darcy) is enclosed by low-permeability barriers (k2), and the system cycle times will nearly exponentially decrease with an increase in permeability (k2) of the low-permeability barrier (Fig. 2). In the calculations of the results shown in Fig. 2, the system cycle times are defined as the number of continuous injection/withdrawal cycles before another gas injection operation is needed to restore the air bubble to the given initial air bubble (i.e., fully saturated air in the k1 region), and the balanced mass cycling schedule is as follow: 12 h of injection at 54 kg/s and 3 h of production at 216 kg/s with 4.5 h of shut-in between injection and production [12], [13].

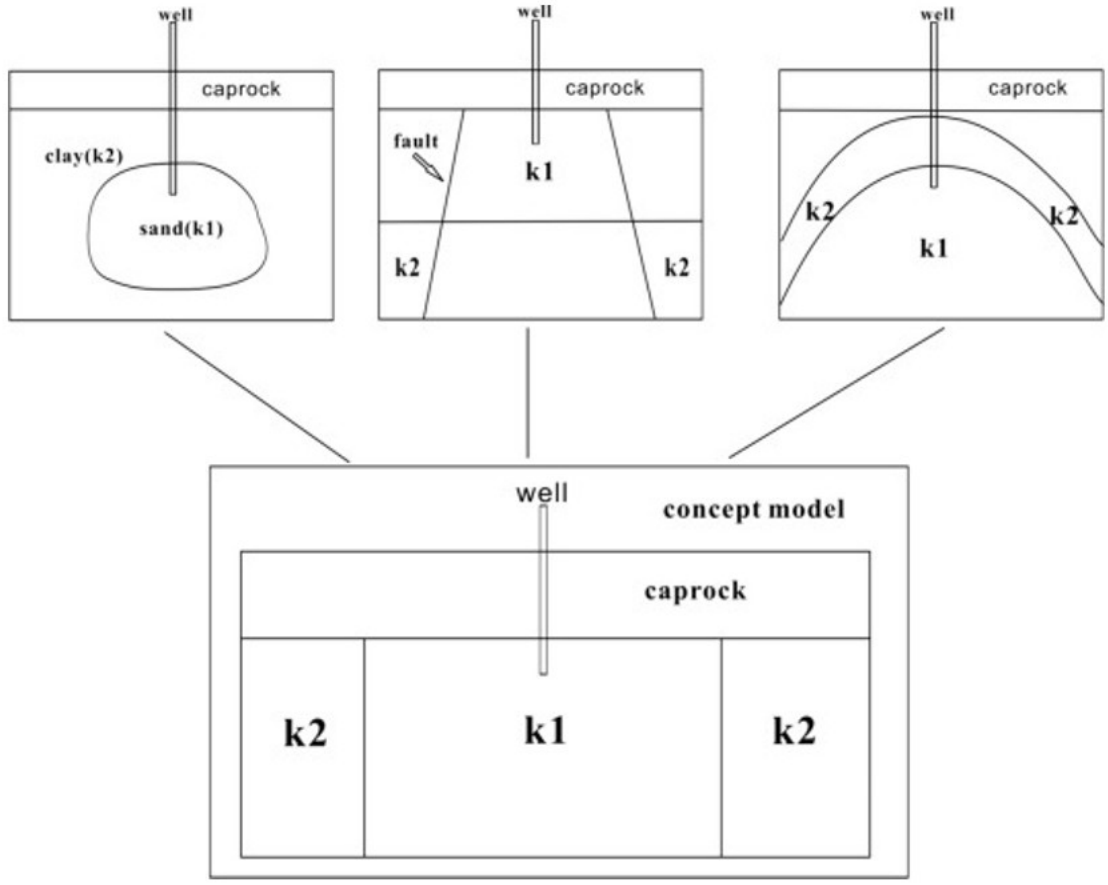

Fig. 1. Natural geological structures with ideal condition for CAESA.

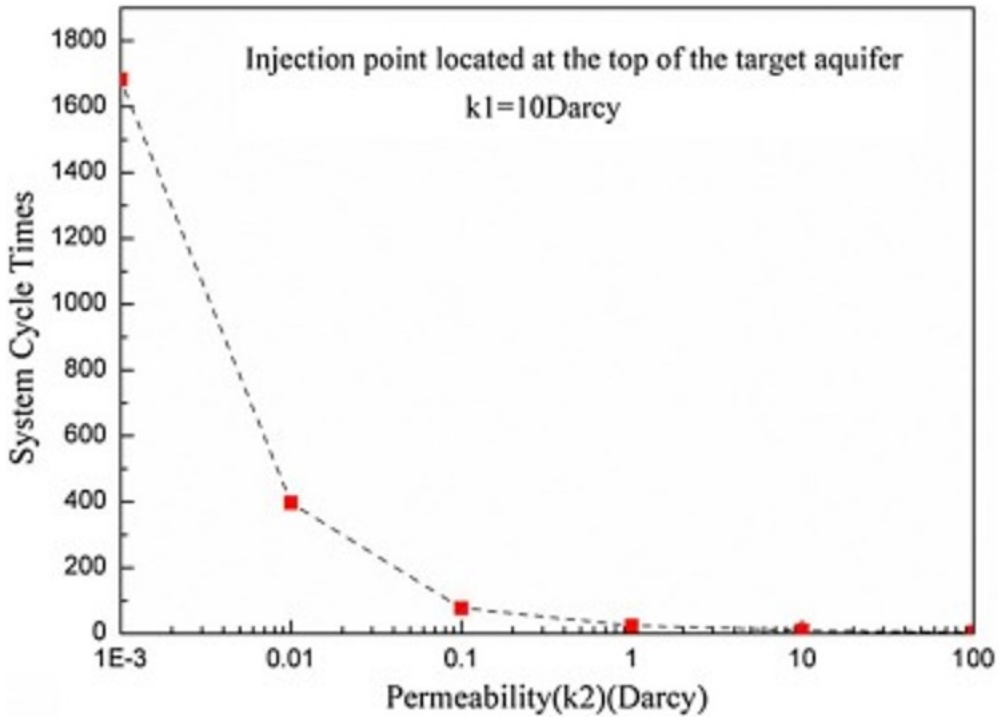

Fig. 2. System cycle times with different barriers (k2).

The results in Fig. 2 show that the permeability in the “barrier” could play a critical role in the performance of CAESA. Naturally, the question is whether we can create a low-permeability barrier to build man-made “wall” in those high-permeability aquifers so that CAESA can be applied successfully to sites without favorable geological structures. In addition, if this technology is feasible for CAESA, more sites can then become available for storage, which would promote development of CAESA. The technology for reforming high-permeability aquifers for the underground natural gas storage and the isolation of contaminant sources was proposed decades ago. Witherspoon et al. [15]proposed the use of a foam barrier in porous media to prevent natural gas flow. The result of their experiment showed that the foam can effectively reduce the permeability of gas and liquid. Pruess and Wu [16] developed the MULKOM simulator for simulating an isothermal gas-water-foam system. Persoff et al. [17] studied the feasibility of the foam barrier using both experimental and numerical simulation approaches. They found that a foam barrier could be effectively formed above the gas-water contact. Moridis et al. [18] investigated the creation of a subsurface barrier to entrap contaminants. A TOUGH2/Gel module was developed for predicting the behavior of gelling fluid and was used to simulate the barrier creation which guided the design of the laboratory experimental [19], [20]. The chemically barrier liquids, such as colloidal silica or polysiloxane, were injected into porous media to create the low-permeability barrier.

The combination of a man-made low-permeability barrier and CASEA in a high- permeability aquifer has not yet been studied and documented in the

previous literatures. We propose the innovative application of man-made low-permeability barriers for CAESA and investigate their feasibility. The relevant questions about this application will be studied in detail, which includes (1) Is it feasible to create low-permeability barrier for CAESA and how does the created barrier affect the performance of CASEA? (2) Which factors are important for a successful barrier creation and how can the factors affect the performance of CAESA?

In this paper, we will use a numerical simulator (TOUGH2/Gel) to investigate the feasibility of building a low-permeability barrier in a highly permeable aquifer to form a favorable structure for aquifer based compressed air energy storage and discuss the energy efficiency improvement. We will also investigate the effects of various factors on the formation of a low-permeability barrier. These results can help us to alter aquifer for improving the performance of CAESA and provide the guidance on the injection grout materials and operation methods for this purpose.

2. Methods

We used TOUGH2/Gel to simulate the low-permeability barrier creation processes and T2Well/EOS3 to simulate the CAES operation with the altered aquifer. TOUGH2 is a numerical simulator for non-isothermal flows of multicomponent, multiphase fluids in porous and fractured media. The flow process is based on Darcy’s law and the variance of component and phase comply with mass and energy balance [19]. TOUGH2/Gel is a TOUGH2 module, which is used for modeling non-isothermal two-phase flow with three components including air, water, and miscible grout in a porous or fractured media [20]. TOUGH2/Gel simulates the low-permeability barrier creation processes as two step processes. In the first step (grout transport), it simulates the transport of grout in the target formation for the given initial and injection conditions. In the second step (solidification), it calculates the porosity and permeability reduction as functions of the local grout concentration at the end of the first step of simulation.

In the simulation of the grout transport, the grout is treated as a component that is miscible in aqueous phase. The liquid phase (i.e., the mixture of grout and water) viscosity is then calculated as a function of the grout concentration based on the given mixing rule (e.g., Power-law mixing rule):

(1)μl=Xlgelμgelb+1-Xlgelμwb-1/b

where the parameter b is suggested to be 0.25 and other parameters are defined in the Nomenclature section. The viscosity of pure grout, μ_{gel}, is assumed to be a simple function of time (Gel Time Curve) by ignoring the detail chemical process of gelation:

(2)μgel=α1+α2·eα3tg/γ

The parameter γ is called scaling factor and is used for stretching the time influence, and the α_1, α_2, α_3 are parameters obtained from an earlier study [20].

In the simulation of solidification process, TOUGH2/Gel assumes that the grout solidifies instantaneously (i.e., no movement during the solidification period). The change in permeability and porosity due to solidification of the grout is calculated based on the final distribution of the grout at the end of the first step of simulation:

(3)ϕ∗=ϕ·(1-A·Sl)

(4)k∗=k·(1-A·Sl)m

(5)AndA=XlgelXcritical

The ratio A measures the degree of solidification. The upper bound of the ratio A is 0.99, which occurs when the grout concentration in liquid phase is larger than 0.99 Xcritical (critical solidification concentration), to avoid the situation of zero porosity which could cause numerical difficulty in the TOUGH2 simulation. Under the condition, the medium is considered to be completely solidified. Otherwise, the medium is incompletely solidified. T2Well/EOS3 is used to evaluate the performance of CAESA in the original aquifer and altered aquifer (the aquifer with a low-permeability barrier simulated by TOUGH2/Gel). T2Well is an integrated wellbore-reservoir simulator [14]. EOS3 is an EOS module that can describe the thermodynamics of H_2O-AIR-HEAT system [19].

3. Modeling the creation of the man-made low-permeability barrier and its impacts on storage performance

In this section, we will first describe the concept model, the numerical grid and the basic parameters used in this numerical modeling study. In addition, we will present three aspects of the simulated results: 1. Grout distribution after the designed barrier creation procedure; 2. The altered permeability and porosity distribution; 3. The impacts of adding the low-permeability barrier on the performance of CAESA, compared to the results of the original aquifer simulation.

3.1. Concept model of the man-made low-permeability barrier

We assume that the target aquifer is a horizontal, uniform, and highly permeable layer that is sandwiched by the impermeable cap rock on top and impermeable underlying basement rock below. The goal is to create a low-permeability barrier in the aquifer around the well and far enough away to keep room for air storage, such as the structure depicted in Fig. 1 (lower panel). The hypothetical procedure would be to first inject a certain volume of the grout such as colloidal silica or polysiloxane, through the well and to then inject enough water through the same well to push the injected grout away from the well so that a high-permeability region around the well would

be enclosed by a low-permeability barrier after the injected grout finally consolidates and seals the critical pore in the formation.

We planned to create a low-permeability barrier approximately 50 m away from the well in a 150 m thick aquifer, which would create the pore storage space of the high-permeability region within the barrier of approximately the same volume as a cavern in the Huntorf plant. To reach this goal, the grout was injected into the aquifer for 10 days at a rate of 50 kg/s and the follow water injection was at a rate of 20 kg/s for 190 days, these rates and durations are estimated based on the piston flow in a radial flow regime.

3.2. The numerical grid and model setup

We created a radial symmetric grid to describe the target aquifer up to 1000 m away from the well and total 800 m thickness geology condition, which target aquifer located at the elevation from −650 m to −800 m with vertical resolution of 5 m and horizontal resolution varying from 0.25 m near well to 70 m at far field (Fig. 3, only 200 m in the target aquifer shown). The stratum above the target aquifer is assumed to be impermeable, and the other model parameters include target aquifer and the character of the injection grout are summarized in Tables 1and 2, respectively. Constant boundary conditions are applied at the far field (1000 m away from the well). The aquifer is initially saturated with water at hydrostatic pressure. The aquifer temperature follows the geothermal gradient of 38.50 °C/km (15 °C at the surface), and the simulations of the barrier creation processes are isothermal. The wellbore is perforated through the entire target aquifer and the wellbore diameter is 0.5 m.

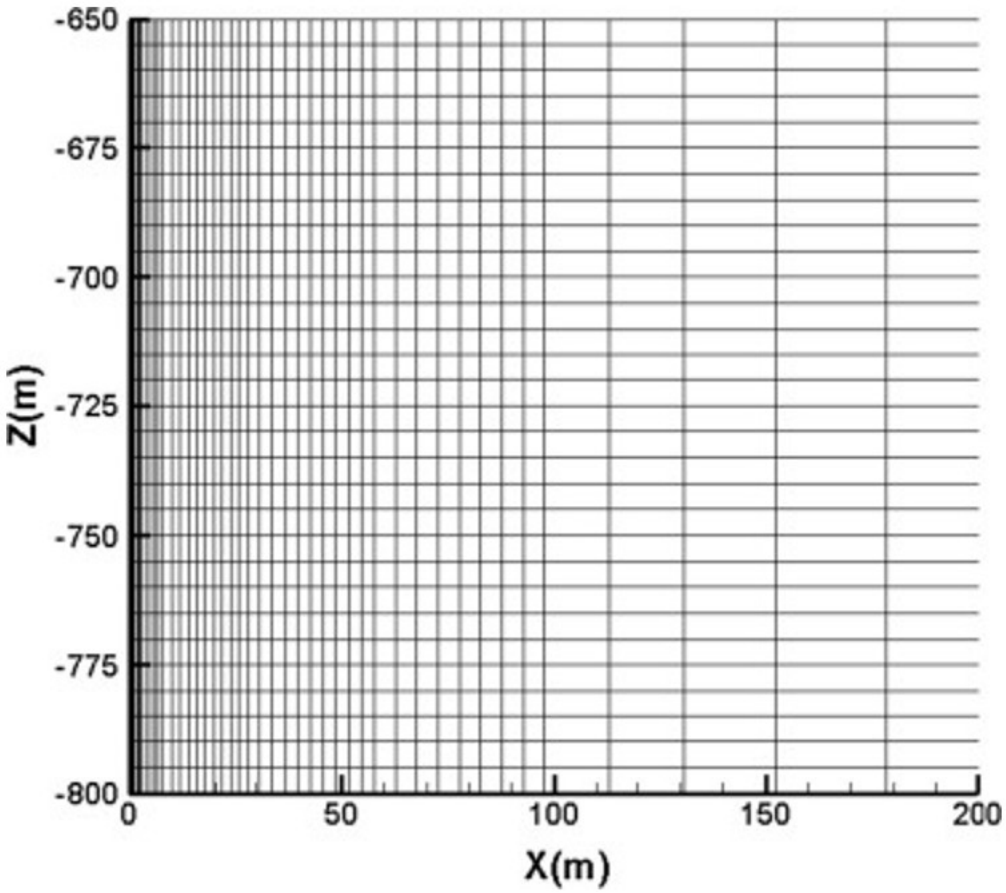

Fig. 3. Profile of a segment of the basic model (200 m in the target aquifer shown).

Table 1. Parameters of the basic model.

Target storage aquifer parameters	
Thickness	150 m
Porosity	0.20
Horizontal permeability	1.00×10^{-11} m^2
Vertical permeability	1.00×10^{-12} m^2
Density of rock	2600 kg/m^3

Table 2. Parameters of the grout used in the basic simulation [20]

Parameters	
Mixing rule	Power-law mixing rule
Permeability reduction	Power-law Permeability Reduction

Parameters	
model	Model
Coefficients of exponential Gel Time Curve	α1 = 3.2235e−3, α2 = 2.8184e−4, α3 = 1.3455e−3
Scaling factor for Gel Time Curve	γ = 600
Density of the grout	998.32 kg/m^3
Exponent of Power-law mixing rule	b = 0.25
Exponent of Power-law Permeability Reduction Model	m = 4.00
Critical solidification concentration	0.12

3.3. Results

3.3.1. Grout concentration distribution

Fig. 4 shows the grout distribution at different times. Over time, the plume of grout is driven away from the well due to the continued injection of water. The injected water can create a grout-free region behind the grout plume. The maximum grout concentration is approximately 0.58, 0.34, and 0.11 at 30 days, 60 days, and 200 days, respectively. Associated with the decreasing maximum grout concentrations, the center of the plume moves to approximately 20 m, 30 m and 50 m at 30 days, 60 days, and 200 days, respectively. The plume increases in size but its peak concentration decreases with the continued injection of water (Fig. 5). Note that the front of the plume is generally more spread out than its tail. This is primarily because of the larger interface area and longer time for grout-water mixing at the plume front than at the plume tail.

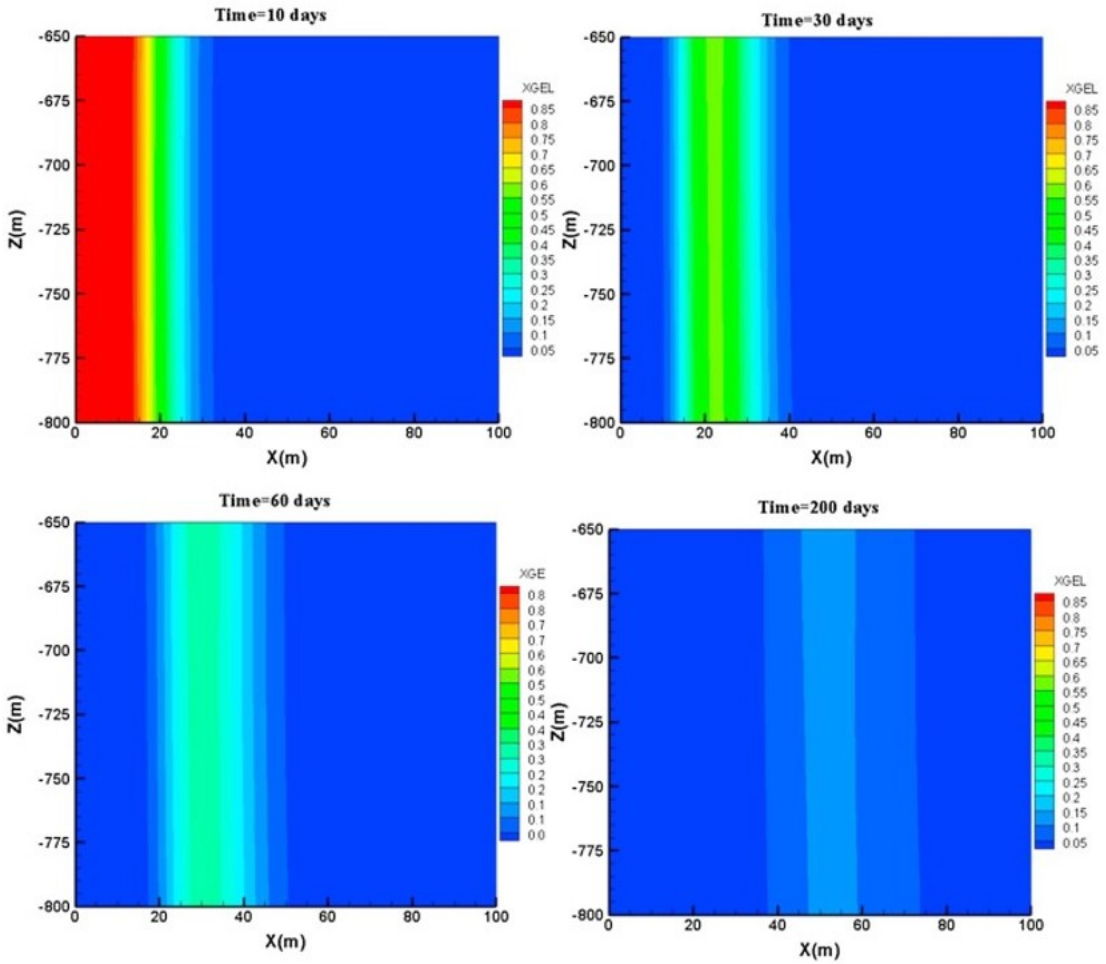

Fig. 4. Grout distribution in different times (10 days, 30 days, 60 days, and 200 days).

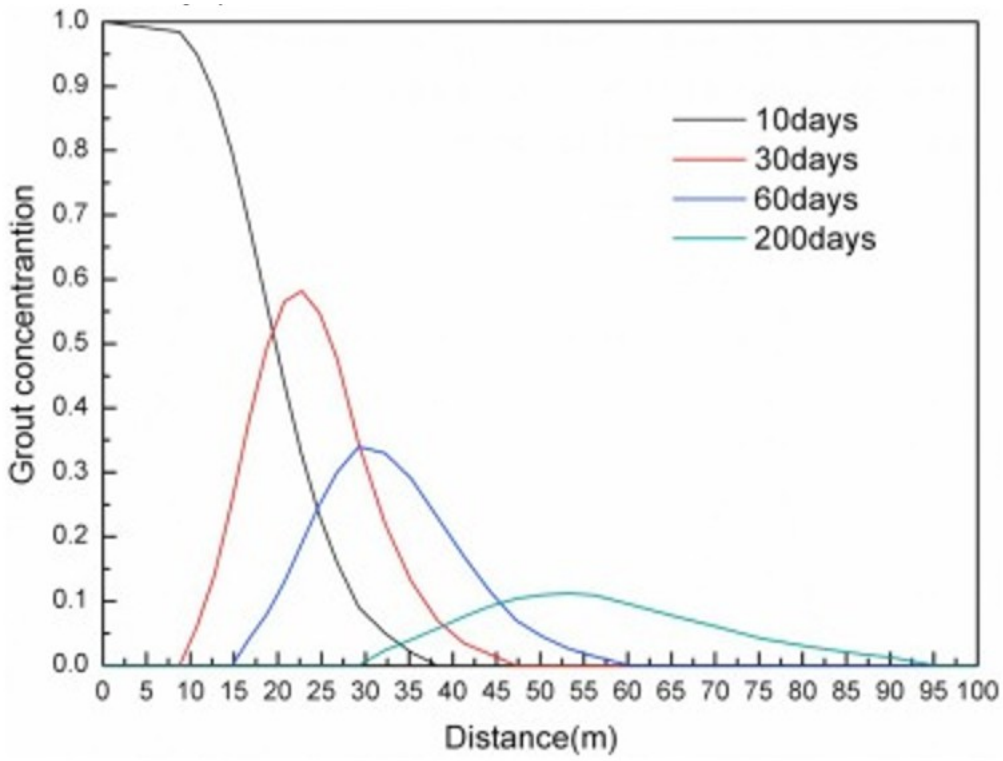

Fig. 5. Grout concentration distribution with distance at different times (−725 m).

3.3.2. The permeability and porosity distribution

Fig. 6 shows the corresponding distributions of permeability and porosity in the altered aquifer after 200 days. The minimal permeability and minimal porosity are both at approximately 50 m away from the well, and permeability and porosity gradually increases to both sides. The permeability at approximately 50 m distance to the wellbore decreases to less than 1 md (1.0×10^{-15} m^2, 1/10,000 of the original permeability), while the permeability within 50 m remains high. The lowest permeability is not located in the center of the altered area, which is consistent with the distribution of the grout concentration (Fig. 5). If the flow was ideal piston flow, we would have an ideal barrier free of spreading. The distance from the wellbore to the inner boundary of the ideal barrier, r_{pi}, can be calculated using the volume balance:

(6)rpi=qwtwρwπhϕ

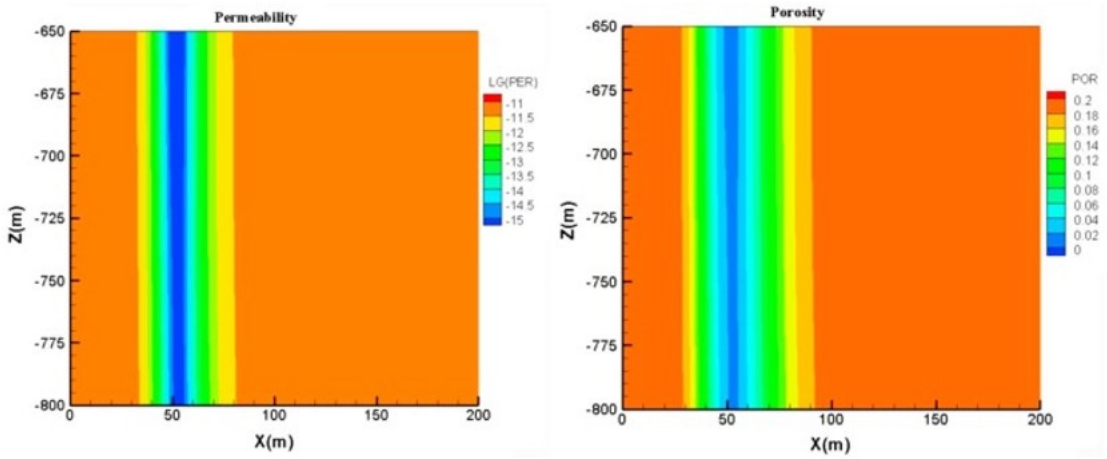

Fig. 6. Permeability and porosity distribution in the altered aquifer.

Similarly, the distance from the wellbore to outer boundary of the ideal barrier, r_{po}, can be calculated as:

(7)rpo=1πhϕqwtwρw+qgtgρg

where the subscripts w and g indicate water and grout, respectively. The other symbols are defined in the Nomenclature section. The distance from the wellbore to the center of the ideal barrier is thus simply the average of r_{po} and r_{pi}.

(8)rbc=0.5(rpo+rpi)

Fig. 7 shows the permeability with distance away from the wellbore at the depth of −750 m. The lowest permeability is located at r_{bl}, which is off the Center r_{bc} and even smaller than the inner boundary of the ideal barrier. This is a result of the uneven spreading of the grout plume during the transportation of the injected grout as shown in Fig. 5. The results show that it is possible to create a low-permeability barrier that encloses a high-permeability region around a well for the use in air storage.

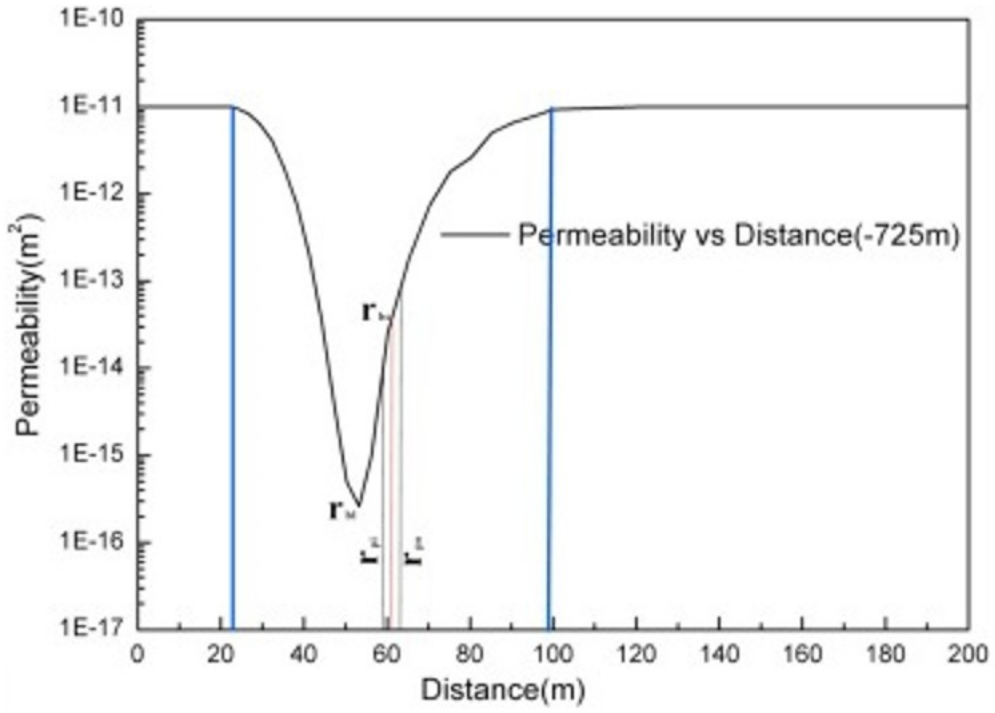

Fig. 7. Permeability with distance away from the wellbore in the altered aquifer (−725 m).

3.3.3. Performance of CAESA within the altered aquifer

To evaluate the impact of the man-made low-permeability barrier on the performance of CAESA, we used T2Well/EOS3 to simulate the system with a hypothetical CAES operation that is similar to the daily cycle operation schedule of the Huntorf plant (injection 54 kg/s × 12 h, shut-in (4.5 h), production (216 kg/s × 3 h) and shut-in (4.5 h) [13], [14]. The initial condition is assumed to be filled with compressed air within 50 m of the wellbore (inside low-permeability barrier) and water outside of this radius, which could be realized by some operations (i.e. water production with air injection) [13]. The same numerical grid as shown in Fig. 3 is used in these simulations, except that the well is extended to land surface. The heat exchange between the fluid in the well and the surrounding formations is calculated using the analytical approach implemented in T2Well. The parameters used in T2well/EOS3 are shown in Table 3. As a comparison, we also simulated the system of the original uniform-permeability aquifer using the same initial conditions and operation schedule.

Table 3. The parameters used in T2well/EOS3.

Wellbore parameters	
Wellbore diameter	0.50 m
Wellbore length	800 m

Wellbore parameters	
Wellbore roughness	4.50×10^{-5} m
Formation thermal conductivity	2.51 W/(m °C)
Parameter of relative permeability and capillary pressure in target aquifer	
Relative permeability model	Van Genuchten-Mualem model
Capillary pressure model	Van Genuchten model
Residual liquid saturation	0.10
Residual gas saturation	0.05
Maximal capillary pressure	5.0×10^{5} Pa
Capillary pressure strength between liquid and gas phases	676 Pa

Energy efficiency is a main concern for compressed air energy storage. Within an entire system, energy efficiency includes three parts: 1. Efficiency of the compression process; 2. Efficiency of the storage process; 3. Efficiency of the expansion to generate electricity. The first and third efficiencies can be improved by utilizing the waste heat (compression heat generated by the compressor and the hot exhaust gases after electricity generation) [1], [21], [22]. Aiming to analyze the performance of the altered target storage aquifer, we focus on the efficiency of the storage process and ignore the efficiency of the compressor, expender and other facilities. Based on the previous studies, the round-trip energy efficiency can be defined as the ratio of energy produced to energy injected through the wellhead in one cycle [11], [13], [23].

(9)Eefficiency=Eproduction/Einjection

Additionally, the ratios of the gas mass production and liquid water production are defined as the ratio of the gas mass or water mass production to the mass of the total production during one cycle.

(10)Rgmass=Mgmass-p/Mtotal-p

(11)Rwmass=Mwmass-p/Mtotal-p

Fig. 8 shows the round-trip energy efficiency, ratio of the gas mass production and ratio of the liquid water production both in the original

aquifer and the altered aquifer at the wellhead through 30 cycles. Within the original aquifer, the energy efficiency quickly decreases from 95% to 64% after 13 cycles mainly because of the increasing liquid water production. This efficiency is stable at approximately 98% within the altered aquifer, in which there is no liquid water produced. In other words, the man-made low-permeability barrier could successfully turn a poor aquifer into an excellent aquifer for CAES, which will be free from the problem of liquid water production and have a small energy leakage rate (similar to the comparison study, in which the efficiency of CAESA (98.7%) is higher than CAESC (96.8%)) [13].

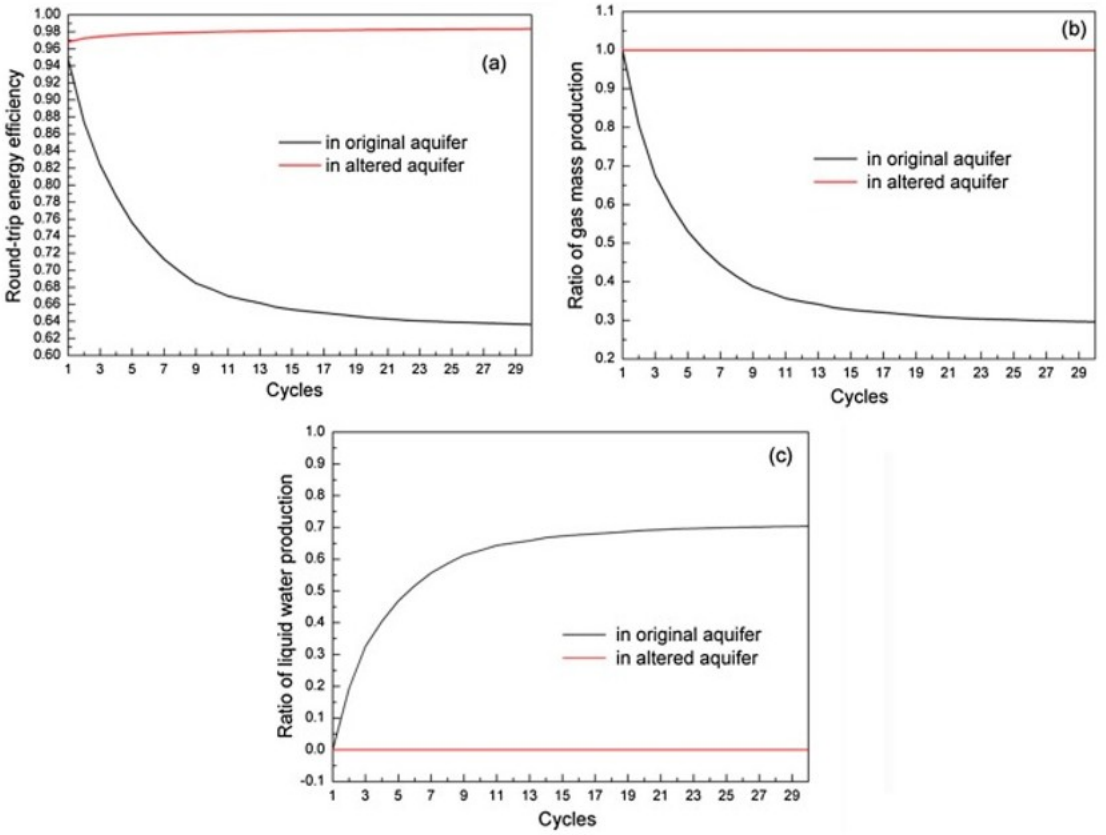

Fig. 8. (a) Round-trip energy efficiency; (b) ratio of gas mass production and (c) ratio of liquid water production in the original aquifer and altered aquifer at the wellhead.

Furthermore, as shown in Fig. 9, during production, the wellhead pressure within the original aquifer drops quickly and decreases to below 4.8 MPa (the maximum pressure difference between the injection and production process is greater than 2 MPa) because the gas quickly escapes to the far field and liquid water invades majority of the perforated section of the well (Fig. 10). Although the injection pressure could drop to below 6.7 MPa because of the low resistance to flow in the aquifer and low pressure in the air bubble, the round-trip storage efficiency drops significantly (Fig. 8). In fact, when the production wellhead pressure drops below the presupposed minimum required pressure, the system has effectively failed. On the other hand, the

low-permeability barrier in the altered aquifer limits the escape of air to the far field and prevents the form of water cone around the well. As a result, only a small volume of air is able to pass the barrier and no liquid water is near the well after 30 cycles (Fig. 10) and both the production pressure and the injection pressure only slightly decrease with time (Fig. 9). It can be expected that only a few percentage of make-up (surplus) injection could keep wellhead pressure within the preferred operation range. Additionally, the pressure distribution at the different stages (after the 30th charge and discharge) in the altered aquifer and original aquifer are shown in Fig. 11. The man-made low- permeability barrier prevents the pressure dissipation in the operation cycle, and the air pressure in the altered aquifer can remain higher than in the original aquifer during the charge and discharge processes. In addition, the high pressure in the altered aquifer can support the available output pressurized air to regenerate electricity.

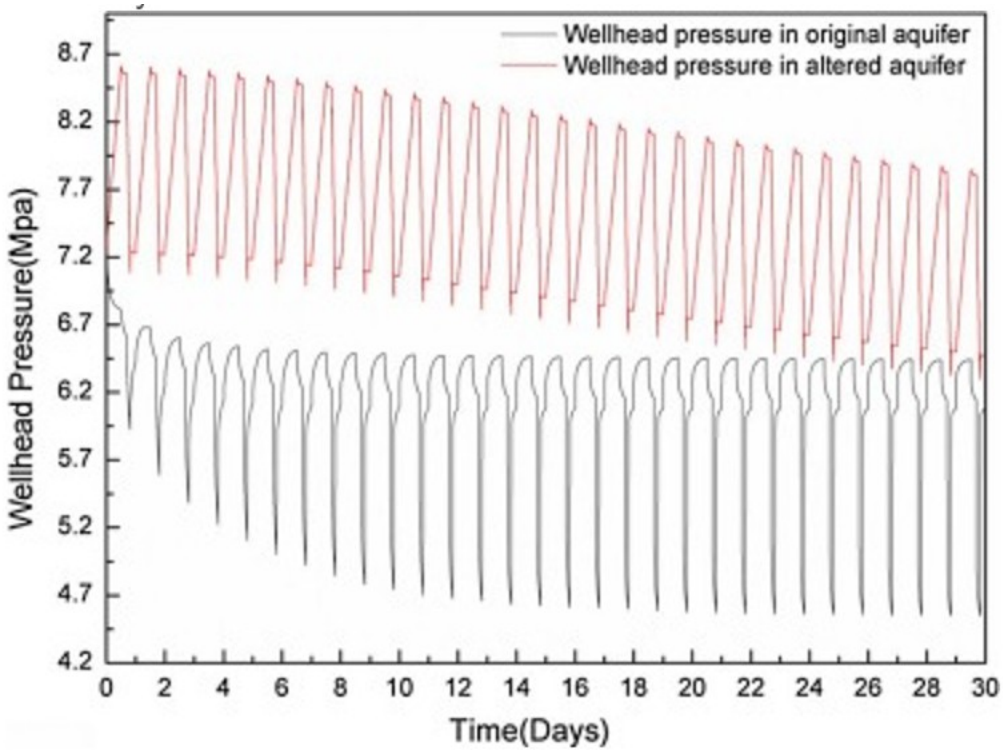

Fig. 9. Wellhead pressure variance in the original and altered aquifer for CAESA.

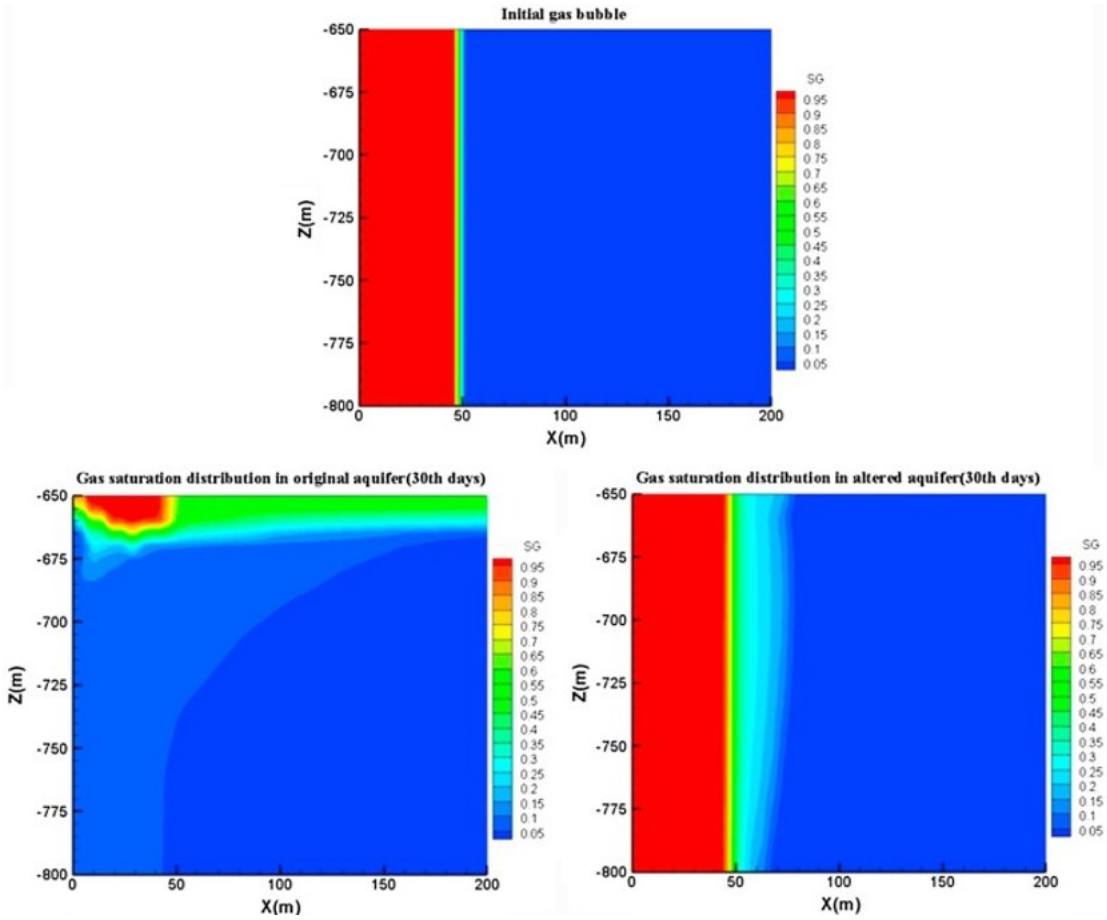

Fig. 10. The initial gas distribution and gas saturation distribution after the 30th cycle, in the original aquifer and altered aquifer for CAESA.

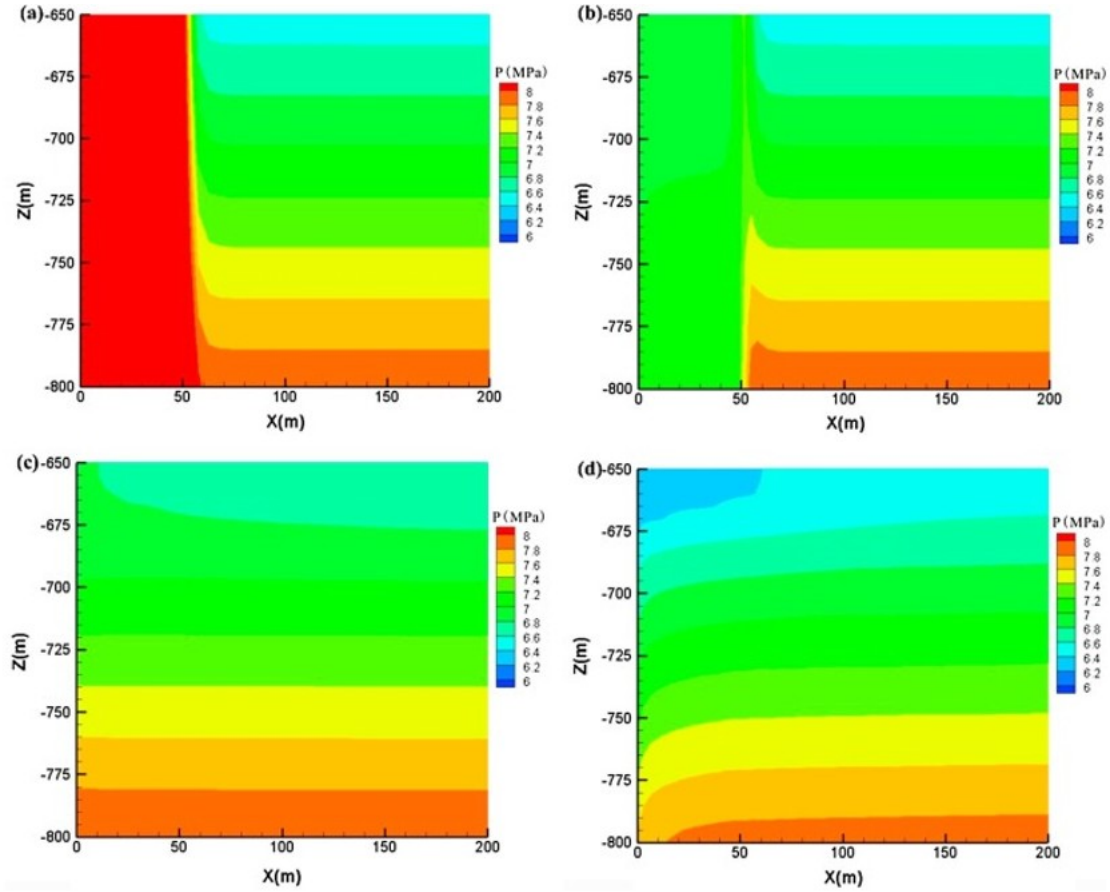

Fig. 11. Pressure distribution at different stages in the altered aquifer and original aquifer; (a) after the 30th charge in the altered aquifer; (b) after the 30th discharge in the altered aquifer; (c) after the 30th charge in the original aquifer; (d) after the 30th discharge in the original aquifer.

The comparison of the CAESA performance between the original and the altered aquifer shows that the man-made low-permeability barrier is effective in the prevention of air loss and formation of water cone and greatly improves the energy storage efficiency in an otherwise unusable aquifer. The results can extend the candidate sites for CAESA and provide a feasible method to alter the aquifer to obtain better energy efficiency.

However, the limitation (two assumption) on the modeling capability offered by TOUGH2/Gel prevents us to study this more realistic issue (possible temporal/spatial scale limitation caused by more complex geochemical reactions of the grouting solution) so that we limit our scope to focus on more fundamental issues of the technology.

Furthermore, the process of injecting grout to create man-made low-permeability barrier would increase the total cost of the operation. Because there is no practical engineering to estimate the increasing cost, we consider the cuttings reinjection cost as a simple analogy analysis. The cost of cuttings reinjection is about 0.025–0.0625 $/kg [24] (assume the density is 10^3 kg/m^{3}and the cost includes the well drilling and other facilities) and it can earn the cost in 155–390 days in our design modeling (about 30% increasing

energy efficiency in altered aquifer comparison with the original aquifer). Also, since no additional wells are required for injecting the grout material, the only additional cost is the injection grout material cost. The total increased cost will be less than the above estimate and the benefit will become more available with the operation continues. Moreover, the technology can extend the candidate sites for CAESA, which can result in more effective wind power plant construction and potential environmental benefits.

4. Influencing factors of creating man-made low-permeability barrier

Many factors affect the creation of the appropriate man-made low-permeability barrier in an aquifer using the gelling process. In this section, we will investigate the effects of these factors using a numerical model. These factors include the critical solidification concentration, the scaling factor of the time-dependence function of grout viscosity, the grout density and rate of the follow- up water injection.

4.1. Critical solidification concentration

The critical solidification concentration (CSC) is an important parameter of the solidification model. As Eqs. (3), (4), (5) show, when the local concentration of grout in liquid phase is greater than the critical solidification concentration, the porous medium would be completely solidified. Otherwise, the solidification is incomplete and only a fraction of the pores would be filled. In this study, three critical solidification concentrations were used (Table 4). All other parameters are the same as in Table 2. Case 1 (CSC = 0.12) is the base case.

Table 4. Critical solidification concentration.

Case	Critical solidification concentration
Case1	0.12
Case2	0.15
Case3	0.20

Because the CSC only affects the solidification process as modeled in TOUGH2/Gel, we will use the same final distributions of the grout that are shown in Fig. 4 to calculate the porosity and permeability alterations. Table 5lists the permeability at the center of the barrier created in the three different cases. The center permeability can reach to 0.2 md, 50 md, 900 md in Case1, Case2, and Case3, respectively. We then simulate the CAES operations for each case with the same schedule and the same initial conditions described above. Fig. 12 shows the round-trip energy efficiency and ratio of gas mass production in the different cases. We have included the performance of the original aquifer (i.e., unaltered) as a reference. As the

critical solidification concentration increases, the round-trip energy efficiency tends to deviate from the base case to the case with the original aquifer simply because the effectiveness of the permeability reduction due to the gelling processes decreases under the same final grout distribution. The main reason for the significant reduction in the round-trip energy efficiency is the occurrence of water cone (Fig. 13). With intermediate permeability reduction (Case 2), the system can keep the same round-trip energy efficiency as the base case for approximately 18 cycles. As the lowest permeability approaches one darcy (Case 3), the man-made barrier effectively fails. Therefore, reducing the center permeability to sub-millidarcy is critical to form a successful man-made low-permeability barrier.

Table 5. The center permeability in the different cases.

Case	**Lowest permeability (m^2)**
Case1	2×10^{-16}
Case2	5×10^{-14}
Case3	9×10^{-13}

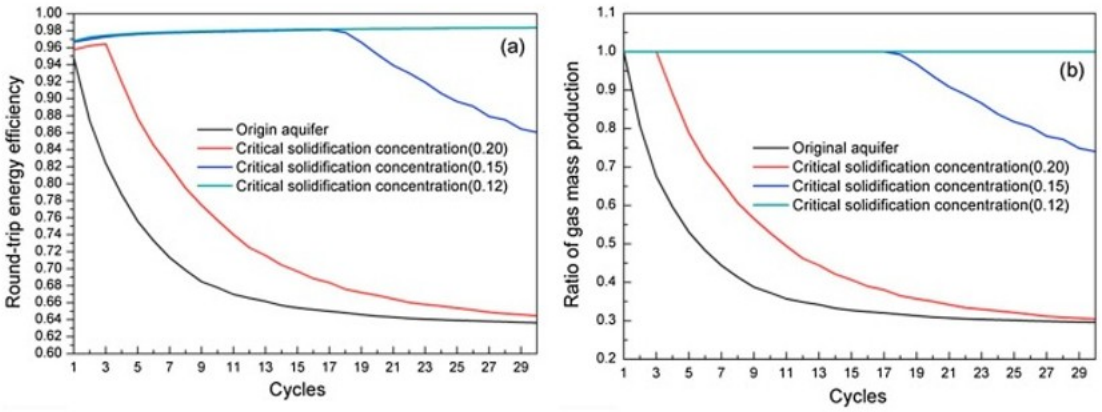

Fig. 12. (a) Round-trip energy efficiency and (b) gas mass flows at the wellhead in the three different altered aquifers and original aquifer.

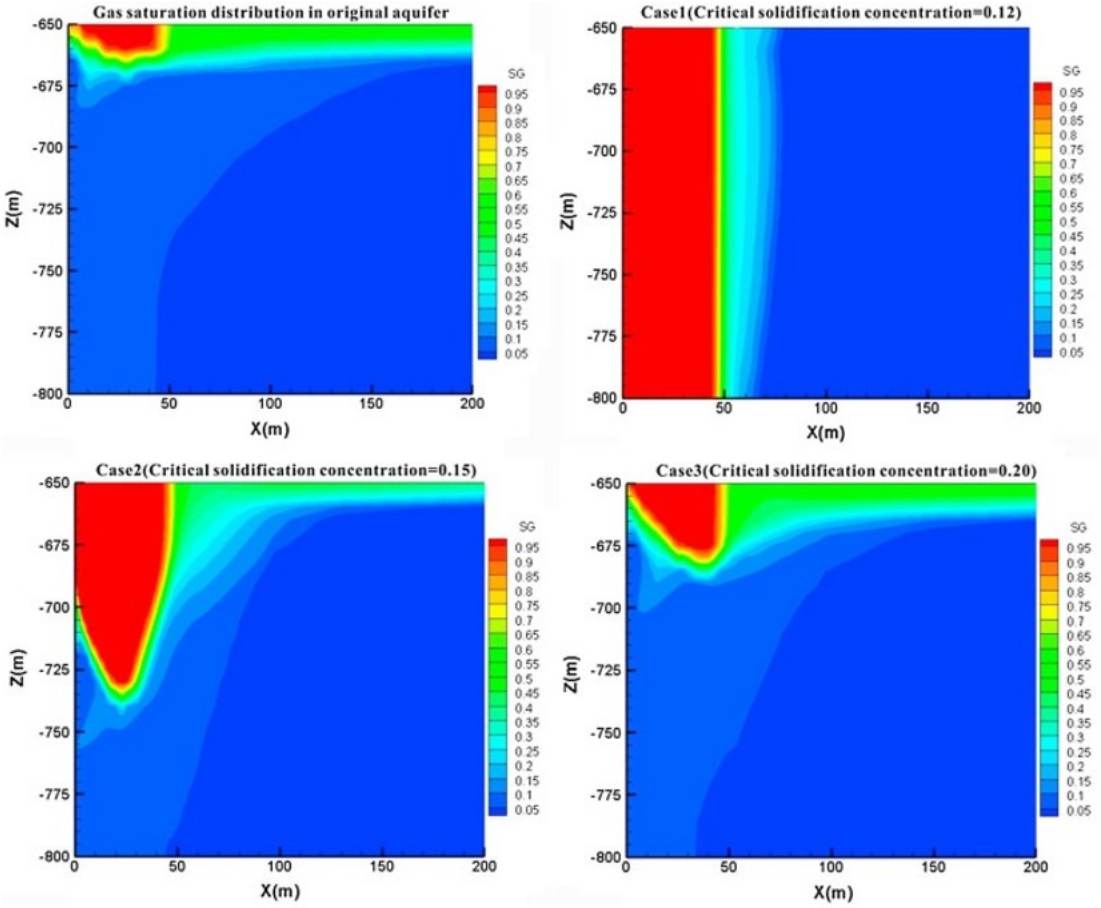

Fig. 13. The gas saturation distribution after 30 cycles in the original aquifer and altered aquifers using different critical solidification concentrations.

When selecting the injection grout material, the results show that the injection grout material with smaller critical solidification concentrations can create better barriers and better energy efficiencies.

4.2. Scale factor of grout viscosity

The viscosity of grout will greatly impact the mobility of the grout contained liquid phase which will determine the final spreading of the grout plume. It is well known that the viscosity of grout will change as a result of complicated gelation processes. In our model, we use a simple time dependent function called Gel Time Curve to calculate the viscosity of the pure grout as shown in Eq. (2). The scale factor of the Gel Time Curve is used to intensify or lessen the time dependence of the pure grout viscosity. For a smaller scale factor, the grout viscosity increases quickly with time and the plume will be harder to move. Five different scale factors (600 for the base case) will be compared and the parameters are shown in Table 6.

Table 6. Scale factors in the different cases.

Case	Scale factor Critical solidification concentration = 0.12
Case1	240
Case2	400
Case3	600
Case4	6000
Case5	∞ (No variance with time)

Table 7 shows the lowest permeability in the altered aquifer of the five different cases. The results show that the smaller the scale factor, the better the barrier. This is because the smaller scale factor leads to a rapid increase of the grout viscosity with time resulting in less mobility of the grout-contained liquid, which allows the grout to stay together. Furthermore, the dependence of the lowest permeability on the scale factor is not linear. The lowest permeability is more sensitive in the cases with smaller scale factors than in the cases with larger scale factors. The results show that the time dependence of viscosity is one of the important factors that need to be considered when selecting the proper material for man-made barrier creation. In addition, in the model, a faster increase of viscosity can result in a barrier with a lower permeability.

Table 7. Lowest permeability of the barrier created in the different cases.

Case	Lowest permeability (m^2)
Case1	1×10^{-19}
Case2	1×10^{-18}
Case3	2×10^{-16}
Case4	2.4×10^{-16}
Case5	2.5×10^{-16}

4.3. Density of grout

If the density of the grout is different from that of ambient water, the injected grout would tend to flow upward or downward in the aquifer, depending on its relative density, because of the buoyancy forces. This tendency of vertical movement of the injected grout would cause an accumulation of grout at the top or bottom of the aquifer layer, which could prevent the formation of a uniform barrier across the aquifer layer. To study

the effects of this factor, we have selected five different grout density cases, including two densities heavier than water, one equal to water (base case) and two lighter than water, as shown in Table 8. The other parameters are the same for the base case.

Table 8. Densities of the injection fluid.

Case	Special gravity (relative to ambient water)
Case1	1.20
Case2	1.10
Case3	1.00 (equal to ambient water)
Case4	0.90
Case5	0.80

Fig. 14 shows the permeability distribution in the five cases with different densities of grout. When the grout density is heavier than water, the grout trends to move down in the aquifer and forms an incomplete permeability barrier. As a result, the barrier looks like a bamboo shoot growing up from the base of the aquifer but dissipates before reaching the top of the aquifer. The case with the grout density lighter than water has the opposite result. The low-permeability barrier hangs down from the aquifer ceiling but does not reach the floor. In both cases, the barrier is not completely formed, as it is in the base case.

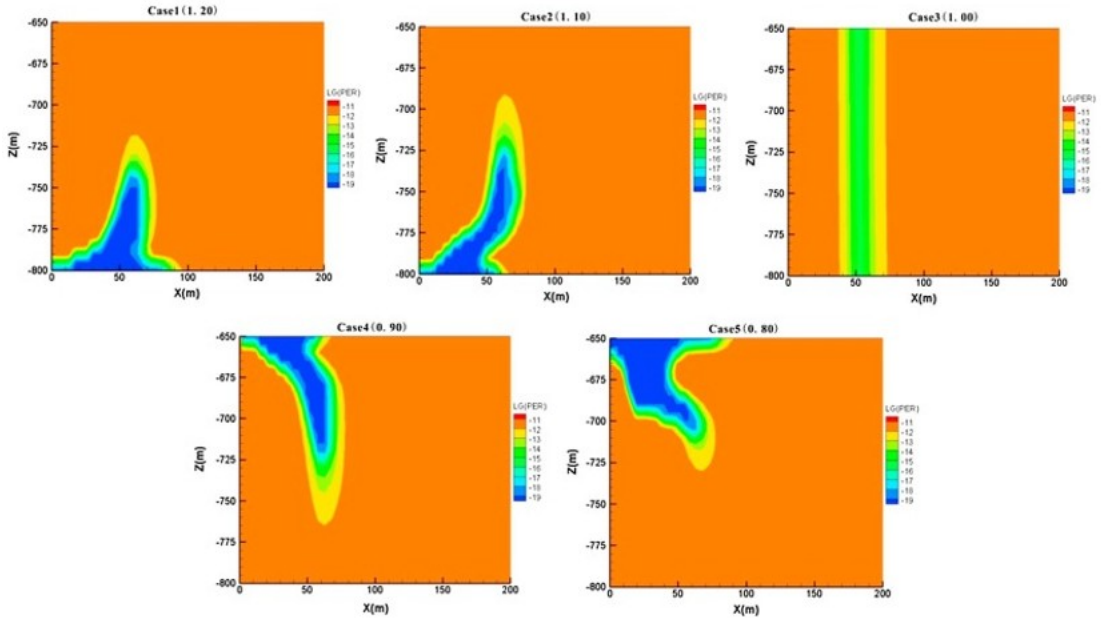

Fig. 14. Permeability barrier with different densities of grout in the aquifer.

To compare the effects of the different barriers shown in Fig. 14 on the performance of CAESA, we performed a set of simulations that have the same initial gas saturation distribution condition and the same daily cycle (injection/production) operations as the base case. Fig. 15 shows the round-trip energy efficiency and ratio of gas mass production in variety of cases. With heavier grout (Case 1 and Case 2), the round-trip energy efficiency is similar to the base case (Case 3) during early simulation times because the barrier in the lower half of the aquifer hinders the inflow of water to the well which tends to flow along the bottom of the aquifer. However, the escape of air through the top half of the aquifer and away from the well is not affected by the barrier in these cases, which causes a quick drop in pressure of the air bubble and invasion of the water into the area around of the well. Of course, the denser the grout is, the worse the results were, in terms of barrier performance. With grout 20% heavier (Case 1), the performance declines down after only 4 cycles, whereas with 10% denser grout (Case 2), it declines after approximately 10 cycles. On the other hand, with less dense grout (Case 4 and Case 5), the barrier is more effective in preventing the escape of air away from the well, which tends to flow along the aquifer ceiling, but less effective in preventing the water invading to the well along the aquifer bottom. As a result, the performance in these cases drop more quickly from the referenced base case than those cases with denser grout but ends at a much higher level of performance than the later because less air leakage tends to sustain the pressure in the air bubble, which in turn prevents the invasion of water (Fig. 16). This is especially true in the case with the grout that is 10% less dense than the base case grout (Case 4), where the performance is only slightly impaired (96% total energy efficiency with 95% gas production).

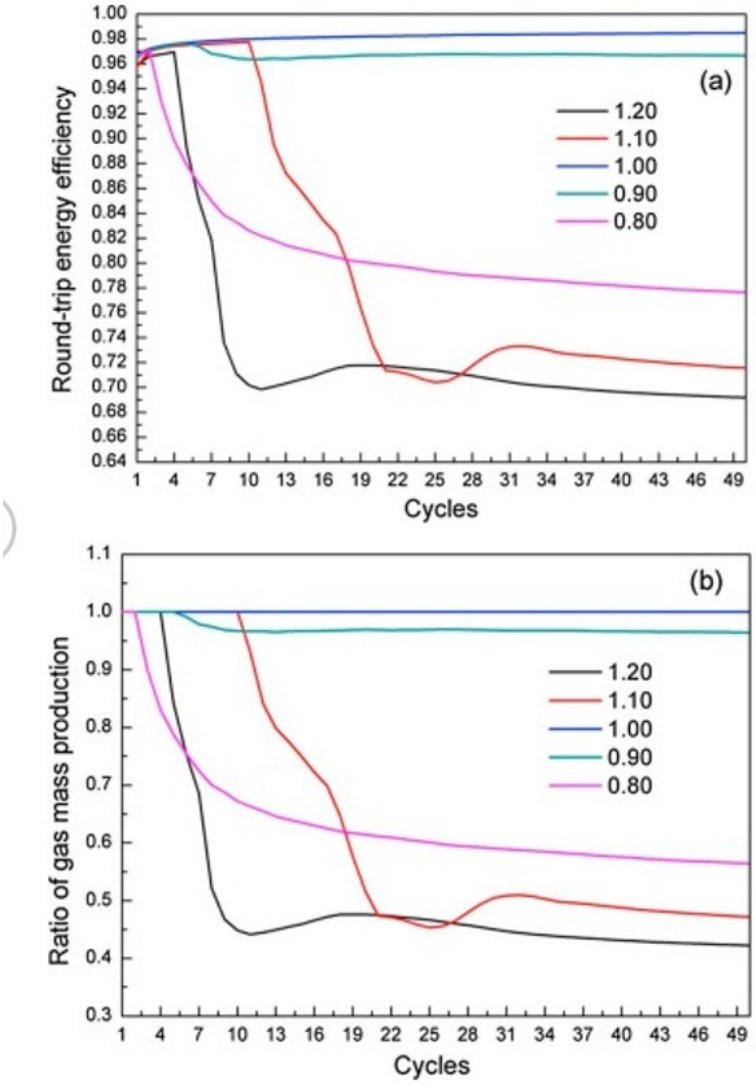

Fig. 15. (a) Round-trip energy efficiency and (b) ratio of gas mass production at the wellhead for the different barriers.

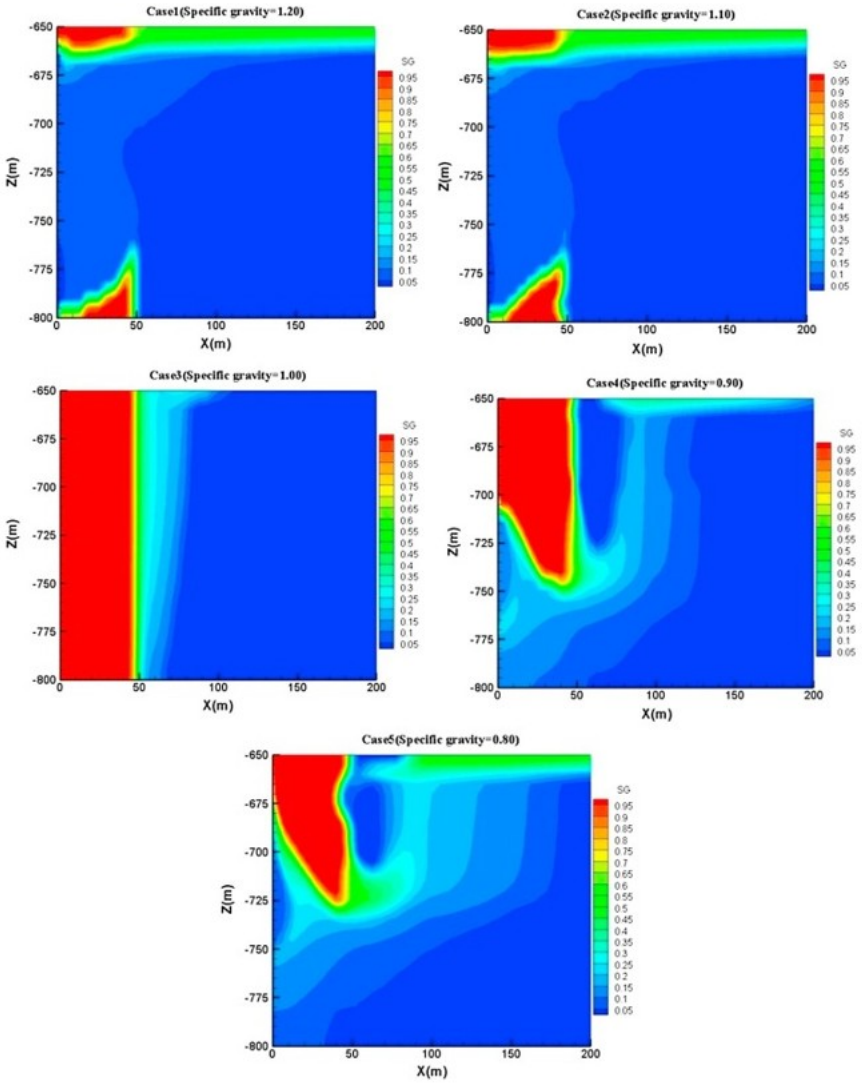

Fig. 16. Gas saturation distribution after 50 days for the different cases.

Note that the initial sharp and vertical gas/liquid interface that results from these simulations is not realistic. The effects of the barrier shape due to the change in relative density of the grout with the development of the initial air bubble would result in very different shapes of the initial air bubble. For example, the lower portion of the aquifer within 50 m in Case 1, may never be saturated with air under normal injection of air through the well because of the small resistance in the upper portion of the aquifer. As a result, the better performance in the early simulation time may not occur at all, in this case. In this sense, an equal grout density or slightly less dense grout (compared to the ambient water or brine) is preferred in the creation of man-made barriers for CAESA simply because the air is much lighter than the water and tends to flow upward. However, if the in situ geological structure is an anticline, the heavier grout may be preferred because it tends to form a lower permeability barrier on the bottom of the aquifer, which pairs well with

the natural geological sealing of an anticline. Of course, if the in situ geological structure is a syncline, lighter grout may be preferred for the a similar reason

4.4. Rate of the follow-up water injection

The follow-up water injection pushes the potential low-permeability barrier away from the well to create enough space for air storage with in highly permeable domain. Generally, with larger volume of water injection, the barrier is pushed farther from the well, which creates a larger volume of high-permeability space available for air storage. This, however, may also dilute the grout too much and the formed barrier would become less effective (i.e., the barrier would have a higher permeability). Meanwhile, the follow-up water injection rate may also play a role in the creation of the man-made barrier. To evaluate these impacts, we have simulated a number of scenarios at three injection rates, 10 kg/s, 20 kg/s, 40 kg/s, for eight different total volumes of water. All scenarios start with the same grout injection of 50 kg/s for 10 days.

Fig. 17(a) shows the square of the distance of the lowest permeability away from the wellbore as a function of the total volume of the follow-up water injection. While the data points representing the various cases are located along a straight line in the plot, they are all significantly below the inner boundary of the theoretical barrier in these simulation scenarios assuming piston flow. In addition, the difference in the trends increases with the increasing total volume of the follow-up water injection. This is the result of the asymmetrical spreading of the grout plume, as described in previous sections (Sections 3.3.1 Grout concentration distribution, 3.3.2 The permeability and porosity distribution). The rate of the follow-up water injection has little impact on the location of the lowest permeability for a given volume of follow up water injected, and differences between the results of the location of the lowest permeability with different injection rates are on the order of only a few meters, which is within the resolution of the grid (5 m). Fig. 17(b) shows the lowest permeability as a function of the volume of the follow up water injection. We also plot the width of the theoretical barrier ($r_{o\text{-}i}$) assuming the piston flow as defined in Eq. (12) (blue[1] line corresponding to the right y-axis).

(12)ro-i=rpo-rpi

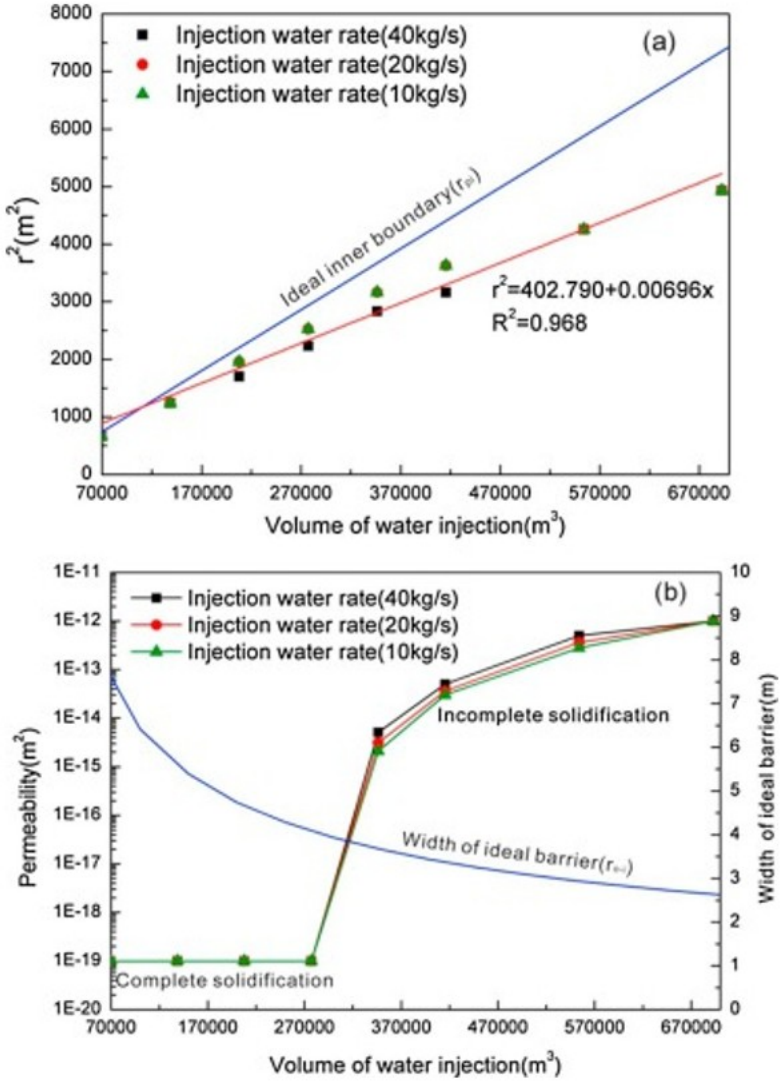

Fig. 17. (a) The distance away from the wellbore of the lowest permeability and (b) the lowest permeability with the different rates of the follow up water injection.

For the given amount of grout injected (50 kg/s for 10 days = 43,200 tons), approximately 322,000 m^3 seems to be the maximum volume of the follow-up water injection that would allow the lowest permeability would exceed 1 md, so the barrier may not be effective. The corresponding width of the theoretical barrier, assuming piston flow, is still approximately 3.7 m. This implies that the mixing of grout and water greatly increase the difficulty in creating an effective barrier. In practice, in engineering design of these barriers, the theoretical width of the barrier estimated using Eq. (12) is a good starting point but detailed numerical simulations with a calibrated model are necessary to design the optimal storage space for CAESA.

The results show that because the injection rate has little impacts on the results, the higher follow-up water injection rates would be preferred considering the time cost to build the low permeability barrier as long as the

bottom hole pressure does not exceed the fracturing pressure or other safety criteria.

5. Conclusions

We have proposed and simulated the creation of man-made low-permeability barriers in high- permeability aquifers. The proposed operation of building a man-made low-permeability barrier to form large-scale energy storage, such as the storage available in Huntorf plant, was validated using TOUGH2/Gel. The asymmetrical porosity and permeability distributions were calculated, and the lowest value reached the acceptable standard. The performances of CAESA including the round-trip energy efficiency, ratio of gas mass production and output pressure, was evaluated for the feasibility of creating man-made low-permeability barriers, which was validated as a method to prevent water coning, keep the energy efficiency high and stabilize the output of high air pressure.

Sensitivity modeling studies were performed to evaluate the impacts of four factors on creating the low permeability barrier, namely, the critical solidification concentration, the time dependency of grout viscosity (i.e., the scale factor of Gel Time Curve), the relative density of the grout, and the follow-up water injection rate and volume. The results can help guide the selection of grout characteristics and optimize the injection schedule for various geological structures and formation properties. The major findings are as follows:

(1) The critical solidification concentration is an important parameter of the grout and control the solidification processes. A smaller critical solidification concentration is generally preferred because it would result in lower permeability in the barrier for an equal grout concentration.

(2) A smaller scale factor of Gel Time Curve is favorable for barrier creation because it would result in a faster increase of the grout viscosity with time which helps the grout to stay together.

(3) The relative density of grout is an important factor that will control the shape of the barrier because of buoyancy forces that may cause an incomplete barrier to form. In a horizontal aquifer, it is better to select a grout with a density close to the in situ water (or brine) density in a horizontal aquifer. For the other geological structures (e.g. anticline or syncline), slightly heavier or lighter grout may be preferred.

(4) For a given volume of grout injected, there is an optimal volume of the follow-up water injection that creates the largest storage space but still keeps the permeability in the barrier low enough to be effective. The rate of the follow up water injection has little impact on the final grout distribution, so that one may choose faster injection rate to finish the creation of a barrier as long as the injection pressure does not exceed some safety criteria.

There remain other problems for creating the low-permeability barriers in CAESA with high-permeability aquifers, which should be studied. The future studies will include improvement of the grout simulation module (the barrier scale may be limited by the more realistic chemical process of gelation and the possible chemical reaction in the aquifer); discussion of the feasibility of directly injecting air to push the grout instead of injection water to create the low-permeability barrier; studies of the initial gas bubble created in different man-made barrier; designs for the experiment using different injection fluid materials, and consider the effectively-hemispherical shell building with wellbore only penetrating the partial thick aquifer.

Acknowledgement

The research was granted by Fundamental Research Funds for the Central Universities through Beijing Normal University (No. 2015KJJCB17). It was also supported by the China Scholarship Council (CSC) for the first author's visit at Lawrence Berkeley National Laboratory. And we thank Stefan Finsterle for providing TOUGH2/Gel.

References

[1] M. Budt, D. Wolf, R. Span, J. Yan**A review on compressed air energy storage: basic principles, past milestones and recent developments**

Appl Energy, 170 (2016), pp. 250-268

[2] Succar S, Williams RH. Compressed air energy storage: theory, resources, and applications for wind power. Princeton Environmental Institute report 2008:8.

[3] D.R. Mack**Something new in power technology**

IEEE Potential, 12 (2) (1993), pp. 40-42

[4] Crotogino F, Mohmeyer KU, Scharf R. Huntorf CAES: more than 20 years of successful operation. Orlando, Florida, USA; 2001.

[5] R. Kushnir, A. Dayan, A. Ullmann**Temperature and pressure variations within compressed air energy storage caverns**

Int J Heat Mass Transf, 55 (21–22) (2012), pp. 5616-5630

[6] M. Raju, S.K. Khaitan**Modeling and simulation of compressed air storage in caverns: a case study of the Huntorf plant**

Appl Energy, 89 (1) (2012), pp. 474-481

[7] E. Barbour, D. Mignard, Y. Ding, Y. Li**Adiabatic compressed air energy storage with packed bed thermal energy storage**

Appl Energy, 155 (2015), pp. 804-815

[8] N. Hartmann, O. Vohringer, C. Kruck, L. Eltrop**Simulation and analysis of different adiabatic compressed air energy storage plant configurations**

Appl Energy, 93 (2012), pp. 541-548

[9] M. Sanchez, A. Shastri, T.M.H. Le**Coupled hydromechanical analysis of an underground compressed air energy storage facility in sandstone**

GeotechnLett, 4 (2014), pp. 157-164

[10] R. Kushnir, A. Ullmann, A. Dayan**Compressed air flow within aquifer reservoirs of CAES plants**

Transp Porous Media, 81 (2010), pp. 219-240

[11] C.M. Oldenburg, L. Pan**Porous media compressed-air energy storage (PM-CAES): theory and simulation of the wellbore-reservoir system**

Transp Porous Media, 97 (2) (2013), pp. 201-221

[12] C. Guo, K. Zhang, C. Li, X. Wang**Modeling studies for influence factors of gas bubble in compressed air energy storage in aquifers**

Energy, 107 (2016), pp. 48-59

[13] C. Guo, L. Pan, K. Zhang, C.M. Oldenburg, C. Li, Y. Li**Comparison of compressed air energy storage process in aquifers and caverns based on the Huntorf CAES Plant**

Appl Energy, 181 (2016), pp. 342-356

[14] L. Pan, C.M. Oldenburg**T2well-an integrated wellbore-reservoir simulator**

Comput Geosci, 65 (2014), pp. 46-55

[15]
P. Witherspoon, S. Benson, P. Pensoff, K. Pruess, C. Radke, Y. WU**Feasibility analysis and development of foam protected underground natural gas storage facilities**

Am Gas Assoc Proc Oper Sec (1987), pp. 539-549

[16] K. Pruess, Y. Wu**On PVT-data, well treatment and preparation of input data for an isothermal gas-water-foam version of MULKOM**

Lawrence Berkeley National Laboratory (1988)

[17] P. Persoff, K. Pruess, S. Benson, Y. Wu, C. Radke, P. Witherspoon, *et al.***Aqueous foams for control of gas migration and water coning in aquifer gas storage**

Energy Sources, 12 (4) (1990), pp. 479-497

[18] G. Moridis, J. Apps, P. Persoff, L. Myer, S. Muller, P. Yen, *et al.***A field test of a waste containment technology using a new generation of injectable barrier liquids**

Lawrence Berkeley National Laboratory (1996)

[19] K. Pruess, C.M. Oldenburg, G. Moridis**TOUGH2 user’s guide version 2**

Lawrence Berkeley National Laboratory (1999)

[20] S. Finsterle, G. Moridis, K. Pruess**A TOUGH2 equation-of-state module for the simulation of two-phase flow of air, water, and a miscible gelling liquid**

Lawrence Berkeley National Laboratory (1994)

[21] N. Hartmann, O. Vöhringer, C. Kruck, L. Eltrop**Simulation and analysis of different adiabatic compressed air energy storage plant configurations**

Appl Energy, 93 (2012), pp. 541-548

[22] Z. Guo, G. Deng, Y. Fan, G. Chen**Performance optimization of adiabatic compressed air energy storage with ejector technology**

Appl Therm Eng, 94 (2016), pp. 193-197

[23] C. Guo, K. Zhang, L. Pan, Z. Cai, C. Li, Y. Li**Numerical investigation of a joint approach to thermal energy storage and compressed air energy storage in aquifers**

Appl Energy, 203 (2017), pp. 948-958

[24] X. Xiang, X. Zhao, T. He, Z. Zhu**Research progress and development tendency of drilling cuttings re-injection technology**

China Offshore Oil Gas, 21 (4) (2009), pp. 267-271

[1] For interpretation of color in Fig. 17, the reader is referred to the web version of this article.